

Enhanced phase-matching for generation of soft X-ray harmonics and attosecond pulses in atomic gases

Vladislav S. Yakovlev^{1*}, Misha Ivanov², Ferenc Krausz^{1,3}

¹*Department of Physics, Ludwig-Maximilians-Universität München, Am Coulombwall 1, D-85748 Garching, Germany*

²*National Research Council of Canada, M-23A, Ottawa, Ontario, Canada K1A 0R6*

³*Max-Planck-Institut für Quantenoptik, Hans-Kopfermann-Strasse 1, D-85748 Garching, Germany*

*Corresponding author: Vladislav.Yakovlev@physik.uni-muenchen.de

Abstract: We theoretically investigate the generation of high harmonics and attosecond pulses by mid-infrared (IR) driving fields. Conditions for coherent build-up of high harmonics are revisited. We show that the coherence length dictated by ionization-induced dephasing does not constitute an ultimate limitation to the coherent growth of soft X-ray (> 100 eV) harmonics driven by few-cycle mid-IR driving pulses: perfect phase-matching, similar to non-adiabatic self-phase-matching, can be achieved even without non-linear deformation of the driving pulse. Our trajectory-based analysis of phase-matching reveals several important advantages of using longer laser wavelengths: conversion efficiency can be improved by orders of magnitude, phase-matched build-up of harmonics can be achieved in a jet with a high gas pressure, and isolated attosecond pulses can be extracted from plateau harmonics.

© 2007 Optical Society of America

OCIS codes: (190.7110) Ultrafast nonlinear optics; (270.6620) Strong-field processes; 999.9999 Attosecond science.

References and links

1. P. B. Corkum, F. Krausz, "Attosecond science," *Nat. Phys.* **3**, 381–387 (2007).
2. M. Hentschel, R. Kienberger, Ch. Spielmann, G. A. Reider, N. Milosevic, T. Brabec, P. Corkum, U. Heinzmann, M. Drescher, F. Krausz, "Attosecond metrology," *Nature* **414**, 509–513 (2001).
3. R. Kienberger, E. Goulielmakis, M. Uiberacker, A. Baltuška, V. Yakovlev, F. Bammer, A. Scrinzi, Th. Westerwalbesloh, U. Kleineberg, U. Heinzmann, M. Drescher, F. Krausz, "Atomic transient recorder," *Nature* **427**, 817–821 (2004).
4. G. Sansone, E. Benedetti, F. Calegari, C. Vozzi, L. Avaldi, R. Flammini, L. Poletto, P. Villoresi, C. Altucci, R. Velotta, S. Stagira, S. De Silvestri, M. Nisoli, "Isolated single-cycle attosecond pulses," *Science* **314**, 443–446 (2006).
5. J. Seres, E. Seres, A. J. Verhoef, G. Tempea, C. Strelci, P. Wobrowski, V. Yakovlev, A. Scrinzi, C. Spielmann, F. Krausz, "Source of coherent kiloelectronvolt X-rays," *Nature* **433**, 596 (2005).
6. A. Gordon, F. X. Kärtner, "Scaling of keV HHG photon yield with drive wavelength," *Opt. Express* **13**, 2941–2947 (2005).
7. J. Tate, T. Augustine, H. G. Muller, P. Salieres, P. Agostini, L. F. DiMauro, "Scaling of wave-packet dynamics in an intense midinfrared field," *Phys. Rev. Lett.* **98**, 013901 (2007).
8. S. Gordienko, A. Pukhov, O. Shorokhov, T. Baeva, "Relativistic Doppler Effect: Universal Spectra and Zeptosecond Pulses," *Phys. Rev. Lett.* **93**, 115002 (2004).
9. G. D. Tsakiris, K. Eidmann, J. Meyer-ter-Vehn, Ferenc Krausz, "Route to intense single attosecond pulses," *New J. Phys.* **8**, 1–20 (2006).

10. K. C. Kulander, K. J. Schafer, J. L. Krause, in *Super-Intense Laser-Atom Physics*, B. Piraux, Anne LHuillier, and K. Rzazewski, eds. (Plenum, New York, 1995), p. 95.
11. P. B. Corkum, "Plasma perspective on strong field multiphoton ionization," *Phys. Rev. Lett.* **71**, 1994–1997 (1993).
12. P. Agostini, L. F. DiMauro, "The physics of attosecond light pulses," *Rep. Prog. Phys.* **67**, 813–855 (2004).
13. T. O. Clatterbuck, C. Lyngå, P. Colosimo, J. D. D. Marin, B. Sheehy, L. F. DiMauro, P. Agostini, K. C. Kulander *J. Mod. Opt.* **50**, 441–450 (2003).
14. T. Fujii, N. Ishii, C. Y. Teisset, X. Gu, Th. Metzger, A. Baltuška, "Parametric amplification of few-cycle carrier-envelope phase-stable pulses at 2.1 μm ," *Opt. Lett.* **31**, 1103 (2006).
15. C. Vozzi, G. Cirmi, C. Manzoni, E. Benedetti, F. Calegari, G. Sansone, S. Stagira, O. Svelto, S. De Silvestri, M. Nisoli, G. Cerullo, "High-energy, few-optical-cycle pulses at 1.5 μm with passive carrier-envelope phase stabilization," *Opt. Express* **14**, 10109–10116 (2006).
16. C. P. Hauri, R. B. Lopez-Martens, C. I. Blaga, K. D. Schultz, J. Cryan, R. Chirla, P. Colosimo, G. Doumy, A. M. March, C. Roedig, E. Sistrunk, J. Tate, J. Wheeler, L. F. DiMauro, E. P. Power, "Intense self-compressed, self-phase-stabilized few-cycle pulses at 2 μm from an optical filament," *Opt. Lett.* **32**, 868–870 (2007).
17. I. P. Christov, M. M. Murnane, H. C. Kapteyn, "High-Harmonic Generation of Attosecond Pulses in the Single-Cycle Regime," *Phys. Rev. Lett.* **78**, 1251–1254 (1997).
18. M. Lewenstein, Ph. Balcou, M. Yu. Ivanov, A. L'Huillier, P. B. Corkum, "Theory of high harmonics generation by low frequency laser field," *Phys. Rev. A* **49**, 2117–2132 (1994).
19. M. Yu. Ivanov, T. Brabec, and N. H. Burnett, "Coulomb corrections and polarization effects in high field high harmonic emission," *Phys. Rev. A* **54**, 742–745 (1996).
20. N. Milosevic, A. Scrinzi, T. Brabec, "Numerical characterisation of high harmonic attosecond pulses," *Phys. Rev. Lett.* **88**, 093905 (2002).
21. P. Antoine, A. L'Huillier, M. Lewenstein, "Attosecond pulse trains using high-order harmonics," *Phys. Rev. Lett.* **77**, 1234–1237 (1996).
22. A. Scrinzi, "Ionization of multielectron atoms by strong static electric fields," *Phys. Rev. A* **61**, 041402R (2000).
23. R. K. Bullough, P. M. Jack, P. W. Kitchenside, R. Saunders, *Phys. Scr.* **20**, 364 (1979).
24. T. Brabec and F. Krausz, "Nonlinear Optical Pulse Propagation in the Single-Cycle Regime," *Phys. Rev. Lett.* **78**, 3282–3285 (1997).
25. M. Spanner, M. Pshenichnikov, V. Olvo, M. Yu. Ivanov, "Controlled supercontinuum generation for optimal pulse compression: A time-warp analysis of nonlinear propagation of ultrabroadband pulses," *Appl. Phys. B* **77**, 329–336 (2003).
26. M. Geissler, G. Tempea, A. Scrinzi, M. Schnürer, F. Krausz, T. Brabec, "Light propagation in field-ionizing media: Extreme nonlinear optics," *Phys. Rev. Lett.* **83**, 2930–2933 (1999).
27. M. B. Gaarde, "Time-frequency representations of high order harmonics," *Opt. Express* **8**, 529–536 (2001).
28. V. S. Yakovlev, A. Scrinzi, "High Harmonic Imaging of Few-Cycle Laser Pulses," *Phys. Rev. Lett.* **91**, 153901 (2003).
29. M. Lewenstein, P. Salières, A. L'Huillier, "Phase of the atomic polarization in high-order harmonic generation," *Phys. Rev. A* **52**, 4747–4754 (1995).
30. Y. Mairesse, A. de Bohan, L. J. Frasinski, H. Merdji, L. C. Dinu, P. Monchicourt, P. Breger, M. Kovačev, R. Taieb, B. Carré, H. G. Muller, P. Agostini, P. Salières, "Attosecond synchronization of high-harmonic soft X-rays," *Science* (302), 1540–1543 (2003).
31. P. Balcou, P. Salieres, A. L'Huillier, M. Lewenstein, "Generalized phase-matching conditions for high harmonics: The role of field-gradient forces," *Phys. Rev. A* **55**, 3204–3210 (1997).
32. M. Geissler, G. Tempea, and T. Brabec, "Phase-matched high-order harmonic generation in the nonadiabatic limit," *Phys. Rev. A* **62**, 033817 (2000).
33. P. Salieres, A. L'Huillier, M. Lewenstein, "Coherence control of high-order harmonics," *Phys. Rev. Lett.* **74**, 3776–3779 (1995).
34. N. B. Delone, V. P. Krainov, *Multiphoton Processes in Atoms* (Springer, Berlin, 2000).

1. Introduction

Attosecond physics has recently been formed as a branch of science that studies attosecond-scale ($1 \text{ as} = 10^{-18} \text{ seconds}$) phenomena by the generation, measurement, and application of attosecond light pulses and electron wavepackets. Even though this discipline is very new, numerous examples of attosecond electron dynamics in atoms, molecules, clusters, and solids have been observed in experiments or addressed theoretically [1]. Even though in some exceptional cases attosecond measurements can be performed without attosecond pulses, for future progress of the field it is of paramount importance to further develop sources of attosecond pulses. Making the pulses shorter, more intense, as well as extending their spectral region would

greatly extend the number of phenomena accessible for experimental observation directly in the time domain or in a time-resolved fashion. This creates demand for a better understanding of the limits of attosecond pulse generation and opportunities, from which novel technologies may benefit. Our paper presents a step in this direction.

Up to the present day, isolated attosecond pulses have only been produced at photon energies $\lesssim 100$ eV [2, 3, 4]. Although generation of harmonic photons with energies as high as 1 keV is feasible [5], generation of sufficiently intense isolated attosecond pulses in the soft X-ray region is hampered by several obstacles: a low efficiency of high-frequency emission at the single-atom level [6, 7], as well as challenges in manufacturing multi-layer coatings capable of reflecting just the cut-off region. As an alternative to gas-phase harmonics, it was proposed to exploit the generation of surface harmonics in the relativistic regime to produce attosecond light pulses [8, 9]. Even though this is a very promising approach that holds potential for increasing the intensity and decreasing the duration of attosecond pulses by orders of magnitude, gas-phase harmonics are likely to remain the workhorse of attosecond experiments in the foreseeable future, since they can be generated at large repetition rates with excellent repeatability, and they do not demand relativistic laser intensities.

In this article we identify several opportunities that appear to offer possible solutions to problems specific to gas-phase harmonics. We show how phase-matching can facilitate the generation of isolated attosecond pulses without the use of measures such as narrow-band spectral filtering or polarization gating. Our theoretical analysis and numerical simulations predict that the efficiency of generation of soft X-ray harmonics is not necessarily limited by the coherence length derived from the different phase velocities of the driving and harmonic waves. Instead, the biggest contribution to the generated harmonic signal usually comes from those parts of the interaction region where conditions of perfect phase-matching are locally satisfied.

The highest (cut-off) energy in the spectrum of high-harmonic radiation is given by [10, 11] $\Omega_{\text{cutoff}}[\text{eV}] \approx W_b[\text{eV}] + 2.96 \cdot 10^{-13} I_L[\text{W}/\text{cm}^2] (\lambda_L[\mu\text{m}])^2$, where W_b is the binding (ionization) potential, I_L is the peak intensity of the driving laser field, and λ_L is its central wavelength. Given that the range of W_b for neutral atoms is very limited, there are two practical options to increase Ω_{cutoff} : increasing the laser intensity I_L or using a longer laser wavelength λ_L . The first option is limited by strong-field ionization. As soon as the laser field ionizes a significant fraction of the atoms, the conversion efficiency of HHG decreases dramatically due to both plasma dispersion and the depletion of the neutral atom response [6]. It is possible to postpone the problem by shortening the laser pulses, but current technology already uses nearly single-cycle pulses and has already reached its limit [5].

The second option to increase Ω_{cutoff} is to increase λ_L [12] (see also pioneering experiments on 'scaled interactions' in Ref. [13]). With advances in optical parametric chirped-pulse amplification, it has recently become feasible to generate powerful phase-stabilized few-cycle pulses in the mid-IR regime [14, 15, 16]. Application of laser wavelengths longer than that of the Ti:Sapphire laser $\lambda_L = 0.8 \mu\text{m}$ was studied theoretically [6, 7], but only at the single-atom level. We combine the analysis of the single-atom response with pulse propagation and uncover the crucial role of propagation effects in this new regime.

2. Modeling HHG in atomic gases

Modeling HHG in a gas jet involves calculation of the single-atom dipole response (SADR) induced by a laser pulse and simulation of co-propagation of the laser and harmonic beams. While the most precise way to calculate the SADR is by numerically solving the time-dependent Schrödinger equation [17], this method is time-consuming. Instead, the Lewenstein model [18] is frequently invoked, which gives qualitatively correct predictions in the regime where the strong-field approximation is valid. We calculated the SADR based on the saddle-point analy-

sis [19, 20] of the Lewenstein model, which has two advantages: it allows the inclusion of arbitrary quasi-static ionization rates and atom-specific recombination matrix elements, and it also provides a convenient tool to study contributions from different electron trajectories independently. In this model, the instantaneous dipole moment of an atom is described as a sum of contributions from different trajectories that lead to a recollision of an electron with the parent ion:

$$d(t) = \text{Re} \left[e^{-i\pi/4} \sum_{\text{trajectories}} a_{\text{ion}}(t) a_{\text{pr}}(t) a_{\text{rec}}(t) \right]. \quad (1)$$

The trajectory-specific probability amplitudes a_{ion} , a_{pr} , and a_{rec} , that represent the ionization, propagation and recombination steps, are defined below. Each trajectory begins at a “birth” moment t_b when an electron is set free by the strong laser field. Depending on this moment, the laser field may remove the electron from the ion once for all, or it may return it back to the ion with a certain kinetic energy W_{kin} . In the latter case, a high-frequency “burst” of harmonics with a photon energy $\Omega = W_b + W_{\text{kin}}$ is generated at the recollision moment [21].

A few trajectories with different values of t_b may lead to a recollision at a given moment t . Regarding a free electron as a classical particle with zero initial velocity, the following relation between the birth and recollision moments can be derived:

$$\int_{t_b}^t A_L(t') dt' = (t - t_b) A_L(t_b), \quad (2)$$

where

$$A_L(t) = - \int_{-\infty}^t E_L(t') dt' \quad (3)$$

is proportional to the vector potential of the driving electric field $E_L(t)$. Henceforth atomic units will be used ($\hbar = e = m_e = 1$) unless stated otherwise.

The first of the probability amplitudes in Eq. (1) is given by

$$a_{\text{ion}} = \left(\frac{dn(t_b)}{dt} \right)^{1/2}, \quad (4)$$

where $n(t_b) = 1 - \exp[-\int_{-\infty}^{t_b} \Gamma(t') dt']$ is the probability that an initially neutral atom is ionized by the moment t_b . The ionization rate $\Gamma(t)$ was calculated numerically in the quasi-static approximation [22]. The propagation and recombination steps are given by

$$a_{\text{pr}}(t) = \left(\frac{2\pi}{t - t_b} \right)^{3/2} \frac{(2W_b)^{1/4}}{|E_L(t_b)|} \exp[-i(t - t_b)W_b - iS(t)] \quad (5)$$

$$a_{\text{rec}}(t) = \sqrt{n(t_r)} \frac{A_L(t_b) - A_L(t)}{[2W_b + \{A_L(t_b) - A_L(t)\}^2]^3}, \quad (6)$$

where $S(t)$ is the action accumulated along a classical trajectory:

$$S(t) = \frac{1}{2} \int_{t_b}^t [A_L(t') - A_L(t_b)]^2 dt'. \quad (7)$$

The pre-exponential terms in Eq. (5) describe the transverse and longitudinal spreading of the electron wave packet. Eq. (6) contains the correction introduced in [6], which takes into account the depletion of the ground state between the moments of ionization and recollision.

We found it very convenient to calculate the dipole response given by Eq. (1) directly in the frequency domain. Since harmonics at a given frequency Ω are radiated in the form of separated

harmonic bursts, this integration can be performed separately for each of them

$$\tilde{d}(\Omega) = e^{-i\pi/4} \sum_{\text{bursts}} \int a_{\text{ion}}(t) a_{\text{pr}}(t) a_{\text{rec}}(t) \exp(i\Omega t) dt = \sum_k \tilde{d}_k(\Omega) \quad (8)$$

with the advantage that each contribution $\tilde{d}_k(\Omega)$, being the Fourier transform of a single harmonic burst k , is a much smoother function of Ω than the full spectrum $\tilde{d}(\Omega)$. Thus, if contributions from different ionization bursts are propagated separately, a relatively low spectral resolution is sufficient to accurately represent the generated harmonic field. For soft X-ray harmonics, this method is much faster than the evaluation of Eq. (1) with the subsequent application of the fast Fourier transform. Additionally, it provides a simple way to track the generation and propagation of different harmonic bursts, which would otherwise require a more complex analysis such as that of time-frequency diagrams [27, 28].

We simulated the propagation of a laser pulse using the slowly-evolving wave approximation (SEWA) [23, 24, 25] adopted for strong-field response [26]. As opposed to the slowly-varying envelope approximation, SEWA is applicable to few-cycle light pulses provided there is negligible reflection of the fields in the medium [24]. Cylindrical symmetry of the light beams reduced the propagation to two spatial coordinates: the propagation coordinate z and the radial coordinate ρ . Further details of the model can be found in [20].

Propagation of harmonics was simulated in the frequency domain, neglecting the small influence of the emerging free electrons on this propagation. In a coordinate system moving with the vacuum speed of light c along the laser axis, the build-up of the harmonic field is described by the following propagation equation (CGS units):

$$\frac{\partial E_{\text{H}}(z, \rho, \Omega)}{\partial z} = \left(-\alpha(\Omega) + \frac{ic}{2\Omega} \nabla_{\perp}^2 \right) E_{\text{H}}(z, \rho, \Omega) + \sum_k s_k(z, \rho, \Omega). \quad (9)$$

Here $\alpha(\Omega)$ is the absorption coefficient of the medium and $s_k(z, \rho, \Omega)$ represents a source term associated with the k -th harmonic burst:

$$s_k(z, \rho, \Omega) = 2\pi i \Omega n_a e a_0 c^{-1} \tilde{d}_k(\Omega), \quad (10)$$

where n_a is the concentration of radiating dipoles, e is the electron charge, a_0 is the Bohr radius.

The most striking feature observed when extremely high-order harmonics are generated by a few-cycle pulse is that efficient generation of a harmonic burst is usually confined to a small part of the interaction region. Fig. 1 illustrates this for two different wavelengths of the driving field: $\lambda_L = 0.75 \mu\text{m}$ and $\lambda_L = 2.1 \mu\text{m}$. In both cases we simulated the propagation of a 1-mJ Gaussian laser pulse, $E_L(t) = E_0 \exp[-2 \log(2) t^2 T_{\text{FWHM}}^{-2}] \cos(\omega_L t - \varphi_{\text{CEO}})$, with the full width at half-maximum (FWHM) equal to two periods of the laser field ($T_{\text{FWHM}} = 4\pi/\omega_L$) and the carrier-envelope-offset (CEO) phase $\varphi_{\text{CEO}} = 0$. The laser beam was focused in a 100-mbar helium jet. The size of the Gaussian beam was chosen to set the initial cut-off energy to 700 eV. During propagation, a laser pulse is de-focused, and possibly, blue-shifted, which eventually lowers the cut-off energy, as it is shown by dashed curves in panels (b) and (d). Although laser propagation was simulated in all spatial dimensions, for this Fig. harmonics were evaluated only on the beam axis. After each propagation step, we saved contributions from trajectories launched within three different half-cycles of the laser pulse. Fig. 1 shows the harmonic output and the single-atom dipole response at 400 eV, contributions from long and short trajectories [29] returning to the parent ion within the same half-cycle of the driving field were added together. In both simulations the intensity of each of the harmonic bursts shows a rapid growth once, or at most, twice, before the cut-off energy drops below the selected harmonic energy. The single-atom dipole responses, which are plotted in panels (b) and (d), reveal that some of

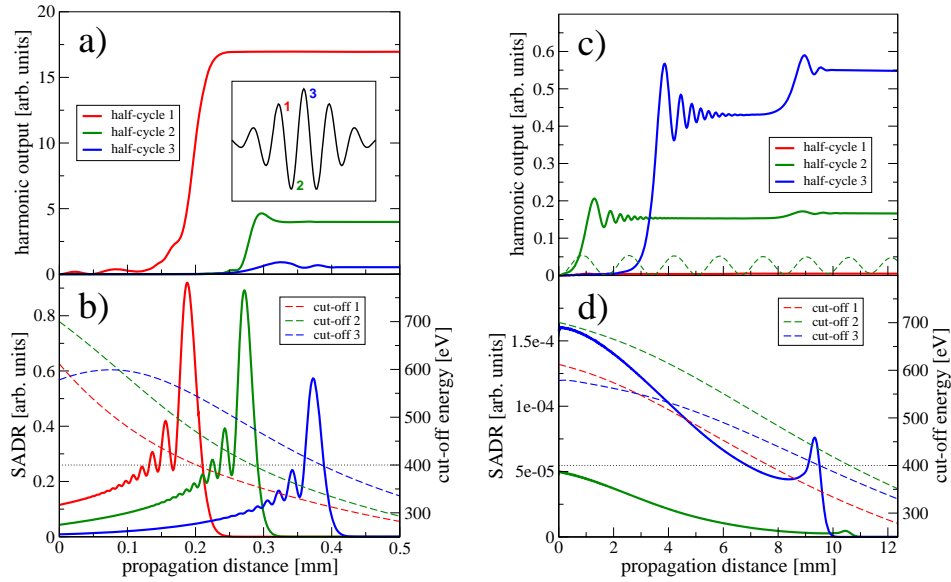


Fig. 1. Contributions from different half-cycles of a 2-cycle laser pulse (inset in panel *a*) to high harmonics at 400 eV. For $\lambda_L = 0.75 \mu\text{m}$, a rapid increase of the harmonic signal (panel *a*) often coincides with a peak of the single-atom dipole response (panel *b*, solid lines). For $\lambda_L = 2.1 \mu\text{m}$ (panels *c* and *d*), the observed highly efficient harmonic generation is due to phase-matching. In both simulations, the cut-off energy was equal to 700 eV at the beginning of propagation; cut-off energies of individual half-cycles are represented by dashed curves in panels *b* and *d*. Harmonic intensity in panels *a* and *c* is measured in the same units, propagation was simulated for a 100-mbar He jet starting from the focus of the laser beam. The dashed green line in panel *c* represents contribution from half-cycle 2 calculated with a non-divergent laser beam. In this case the harmonic generation is not phase-matched and a regular coherent ringing is observed.

the regions of this highly effective harmonic generation coincide with a local increase of the SADR. This increase is observed when the cut-off energy of a particular half-cycle becomes close to the selected harmonic energy, and it is caused by two factors: a reduced energy chirp of the returning electron wavepacket (see Section 4) and a weaker depletion of the ground-state. The latter factor played a more important role for $\lambda_L = 0.75 \mu\text{m}$, since the initial laser pulse ionized more than 50% of the atoms.

Qualitative behavior for $\lambda_L = 2.1 \mu\text{m}$ (panels (c) and (d) in Fig. 1) is remarkably different from the one observed with the smaller driving wavelength. In this case, the local increase of the SADR cannot explain the sudden build-up of harmonic bursts. For $\lambda_L = 2.1 \mu\text{m}$, the ground-state depletion is negligibly small, since a much lower laser intensity is required to generate harmonics with the same cut-off energy: the probability of ionization by the two-cycle pulse was less than 0.2%. As we will show in the next section, in this regime the fast build-up of harmonic bursts is explained by self-phase-matching, which can become very efficient for one of the bursts.

The observed formation of harmonic bursts provides a key to the generation of isolated attosecond pulses at photon energies approaching or even exceeding 1 keV. Since different harmonic bursts require different conditions for their efficient generation, it is possible to find such conditions that one burst completely dominates all other bursts, even if harmonics are generated in the plateau region. While this does not completely obviate the necessity to apply spectral fil-

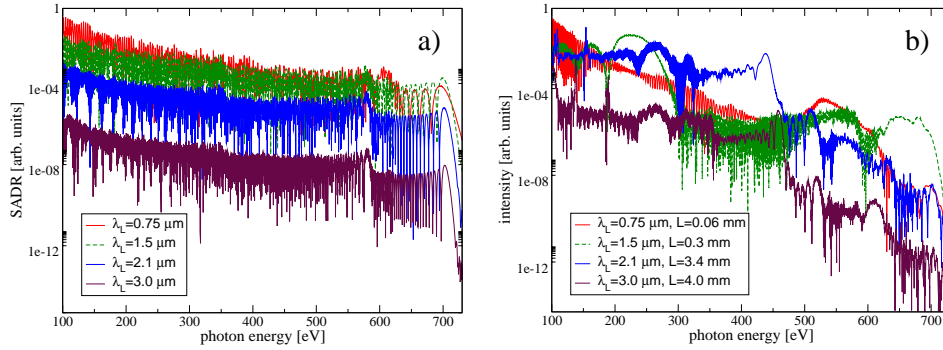


Fig. 2. Single-atom dipole response at the beginning of a 100-mbar He jet (a), and the far-field spectral intensity of high harmonics (b) generated by a 1-mJ 2-cycle pulse for different values of the laser wavelength λ_L . In each simulation, the initial semi-classical cut-off energy was equal to 700 eV and the jet thickness L was chosen to reduce it by 10% (legend in panel *b*).

tering in order to generate a single attosecond pulse, it may significantly relax requirements on such a filter, since no careful selection of the cut-off region is required.

To illustrate how a single attosecond pulse can be generated far from the cut-off region, and also to illustrate the role of propagation effects in the scaling of HHG with the wavelength of the driving field, we made a series of 3D simulations, the main inferences from which are presented in Fig. 2. This Fig. shows single-atom dipole responses (a) and far-field harmonic spectra originating from the atomic ensemble (b) for different values of the central laser wavelength λ_L . Similarly to the simulations shown in Fig. 1, the input laser pulse was a 1-mJ two-cycle Gaussian one. Unlike the previously demonstrated simulations, we calculated the radial distribution of harmonics and propagated them in all spatial dimensions. The gas medium was terminated as soon as Ω_{cutoff} was reduced by 10% of its initial value, which was equal to 700 eV in all the simulations.

Comparing the two panels of Fig. 2, we see that in spite of the fact that the SADR decreases as λ_L is increased, it still may be beneficial to increase the wavelength of the driving field to maximize the output from the ensemble of atoms. This will be further discussed in the following sections. We also observe that the far-field on-axis harmonic intensity does not always show modulations in the plateau region. If one such region can be isolated by means of spectral filtering, a single attosecond pulse can be generated. An example is shown in Fig. 3. Transmission of harmonics generated with $\lambda_L = 1.5 \mu\text{m}$ through $0.1 \mu\text{m}$ of Cu and $0.1 \mu\text{m}$ of Pd suppresses harmonics below 100 eV, thereby isolating the hump around 230 eV. As a result, an isolated 60-attosecond pulse is extracted from harmonics in the far field (Fig. 3b), which confirms that one of the trajectories contributed under exceptionally favorable phase-matching conditions.

3. Phase-matched generation of soft X-ray harmonics

Analysis of the role of phase-matching in HHG is often based on the concept that every harmonic order can be assigned a certain phase [30]. As the duration of the driving pulse approaches the single-cycle limit, this concept loses its validity, since the few harmonic bursts generated by the laser pulse may have very different amplitudes, durations, and phases. Instead of narrow harmonics at odd multiples of the laser frequency the spectrum of the generated high-frequency radiation may show rather irregular spikes that result from the interference of different trajectories. Not only generation, but also propagation conditions for different harmonic

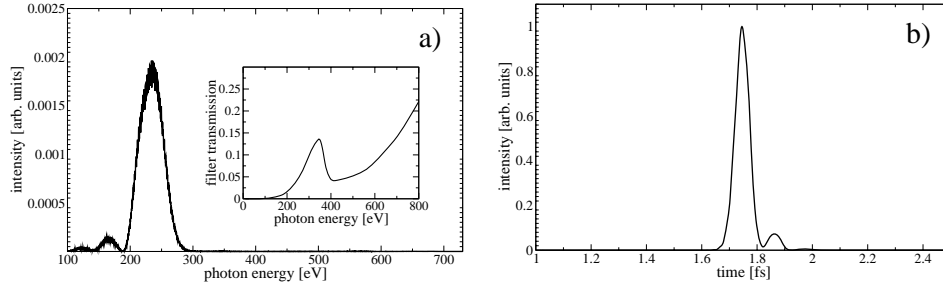


Fig. 3. Generation of a single attosecond pulse in the plateau region. Panel *a* shows the far-field on-axis harmonic signal generated with $\lambda_L = 1.5 \mu\text{m}$ (green dashed line in Fig. 2b) after it was transmitted through a filter made of $0.1 \mu\text{m}$ of Cu and $0.1 \mu\text{m}$ of Pd. The filter suppresses harmonics below 100 eV, its transmittance is shown by the inset in panel *a*. Panel *b* shows the time-domain intensity of the harmonic field after the filter.

bursts may differ significantly. Therefore, phase-matching should be separately investigated for each contributing electron trajectory.

Phase-matching conditions for a selected harmonic burst k are determined by the phase of the corresponding source term s_k in Eq. (9). This phase can be approximately calculated using the stationary phase method to perform the Fourier transform of the SADR [29, 31]:

$$\arg[s_k] \approx \varphi(t_r^{(k)}) = \Omega t_r^{(k)} - S(t_r^{(k)}) - (t_r^{(k)} - t_b^{(k)}) W_b + \frac{\pi}{2}, \quad (11)$$

where the birth moment t_b and the recollision moment t_r of the k -th trajectory are supposed to be chosen such that

$$\Omega = W_b + W_{\text{kin}} \quad (12)$$

is satisfied in addition to Eq. (2) for the selected emission frequency Ω . To simplify the notation we will omit the index k , but our consideration is still limited to one selected harmonic burst. As the laser pulse changes during propagation, the values of t_b and t_r have to be adjusted in order to keep conditions (2) and (12) fulfilled. Consequently, t_b and t_r are functions of the propagation coordinate z . A change of the phase φ with z leads to a phase mismatch. Differentiating Eq. (11) we obtain

$$\frac{d\varphi}{dz} = \Omega \frac{dt_r}{dz} - \frac{dS}{dz} - \left(\frac{dt_r}{dz} - \frac{dt_b}{dz} \right) W_b. \quad (13)$$

The generation of harmonics is most efficient when $d\varphi/dz$ becomes equal to zero—in this case, contributions from all atoms interfere constructively, and the intensity of the generated radiation grows quadratically with the number of contributing dipole emitters. Eq. (13) can be simplified with the aid of Eqs. (2) and (7):

$$\frac{d\varphi}{dz} = W_b \frac{dt_b(z)}{dz} - \frac{\partial S}{\partial z} = W_b \frac{dt_b(z)}{dz} - \int_{t_b(z)}^{t_r(z)} dt [A_L(z, t) - A_L(z, t_b(z))] \frac{\partial A_L(z, t)}{\partial z}, \quad (14)$$

where the derivative $\partial S/\partial z$ is calculated for fixed t_b and t_r .

There are two sources of phase-mismatch, both of which are described by Eq. (14). First, if the laser pulse and harmonic radiation have different phase velocities, the driving field experiences a shift in the co-moving coordinate frame as the pulses propagate. Second, any distortion of the laser pulse during its propagation—a change of its intensity, frequency or the CEO phase—makes an additional contribution to the phase of the emitted harmonics by affecting

the phase of the recolliding wave packet. These two sources of phase mismatch often have opposite signs, so that they can compensate each other. This was first demonstrated in a regime where a few-cycle pulse ionizes a significant fraction of atoms [32], which results in an increase of its instantaneous frequency (blue-shift). This mechanism is referred to as the non-adiabatic self-phase-matching (NSPM) and it leads to a rapid growth of the harmonic signal. However, it has not been widely recognized that this kind of perfect phase-matching can also be achieved with moderate ionization rates, where the blue-shift of the laser pulse can be neglected. Here we show that it is not only possible with realistic parameters, but also the importance of this mechanism grows with the harmonic order, so that for sufficiently high-order harmonics the conversion efficiency is no longer determined or limited by the coherence length, but by the length over which the condition $d\varphi/dz = 0$ is approximately satisfied.

In order to investigate how a single harmonic burst is built up, it is sufficient to consider one single cycle of the driving field. As long as the instantaneous frequency of the laser pulse remains constant, propagation of a selected field oscillation can be approximately described by specifying how its amplitude and position in the co-moving system of coordinates depend on the propagation distance. This is incorporated into the following ansatz:

$$A_L(z, t) = f(z)g(t - \tau(z)), \quad (15)$$

$$E_L(z, t) = -f(z)g'(t - \tau(z)), \quad (16)$$

where the electric field $E_L(z, t)$ is obtained from Eq. (15) by making use of Eq. (3). Let us now insert this ansatz into Eq. (14). Trajectories that significantly contribute to HHG start in the vicinity of a peak of the electric field, where the ionization rate is highest. Therefore a change of the amplitude of the laser field has little influence on t_b , so that dt_b/dz is approximately equal to $d\tau/dz$. With this approximation we obtain the following simple formula that determines phase-matching conditions for a selected harmonic burst:

$$\frac{d\varphi}{dz} = \Omega\tau'(z) - \frac{2f'(z)}{f(z)}S(t_r(z)). \quad (17)$$

Perfect phase-matching is achieved when

$$\frac{2f'(z)}{f(z)} \frac{1}{\tau'(z)} = \frac{\Omega}{S(t_r(z))}. \quad (18)$$

In analogy with NSPM, we refer to this regime as self-phase-matching (SPM).

Condition (18) is consistent with the well-known fact that high harmonics are generated most efficiently when a gas jet is placed behind the laser focus [33]. Indeed, the plasma dispersion and the Gouy phase shift increase the phase velocity of the laser pulse, so that $\tau'(z)$ becomes negative. In this case, Eq. (18) can only be satisfied if $f'(z) < 0$, that is, the amplitude of the laser field must decrease during propagation. We have to recognize, however, that not only a decrease of the laser intensity leads to $f'(z) < 0$, but also a change of the CEO phase of a few-cycle pulse can significantly decrease the amplitude of a selected laser cycle in a few-cycle pulse.

Let us now investigate the right-hand side of Eq. (18). The ratio Ω_{cutoff}/S scales as the laser frequency $\omega_L = 2\pi c/\lambda_L$. For a monochromatic laser field, it is possible to show that only trajectories for which $0.28 < \Omega/(S\omega_L) \leq 2.2$ can contribute to harmonics with a frequency $\Omega \geq \frac{1}{2}\Omega_{\text{cutoff}}$. A requirement that the phase-matched trajectory be a short one narrows this interval yet further: $0.96 \leq \Omega/(S\omega_L) \leq 2.2$. Thus, as a rough estimate, condition (18) can be satisfied in the upper part of the plateau region if

$$\frac{2f'(z)}{f(z)} \sim \tau'(z)\omega_L. \quad (19)$$

For example, if a 0.75- μm laser pulse ionizes 1% of atoms in a 100-mbar gas jet, then the plasma dispersion alone leads to $\tau'(z) = 0.04$ fs/mm. According to Eq. (19), the intensity of the selected laser cycle must decrease by approximately 10% per mm of propagation. Such a drop in intensity is often observed in HHG experiments and simulations.

Whenever Eq. (18) is satisfied, the harmonic output rapidly grows with z over a distance L_{eff} , which we call the effective length of coherent harmonic build-up. This distance may be limited by a drop of the SADR caused by a decrease of the laser intensity, but in most cases the main limiting factor is dephasing caused by a non-zero second derivative of $\varphi(z)$ at a position z_0 , where perfect phase-matching $\varphi'(z_0) = 0$ is achieved:

$$\varphi(z) \approx \varphi(z_0) + \frac{1}{2} \varphi''(z_0)(z - z_0)^2. \quad (20)$$

In this case it is reasonable to define L_{eff} by $|\int_{-\infty}^{\infty} s(z_0) \exp(i\varphi(z)) dz| = L_{\text{eff}} |s(z_0)|$, which yields

$$L_{\text{eff}} = \left(\frac{2\pi}{|\varphi''(z_0)|} \right)^{1/2}. \quad (21)$$

The second derivative $\varphi''(z_0)$ can be evaluated using Eqs. (14), (17), and (18):

$$\varphi''(z_0) = \Omega \tau''(z_0) - \Omega \tau'(z_0) \left(\frac{f''(z_0)}{f'(z_0)} - \frac{f'(z_0)}{f(z_0)} \right) - W_b \frac{2f'(z_0)}{f(z_0)} \tau'(z_0). \quad (22)$$

In order to estimate L_{eff} , we neglect the second derivatives $f''(z_0)$ and $\tau''(z_0)$ in the above expression and assume that $\Omega \gg W_b$. Together with Eq. (19) this yields

$$L_{\text{eff}} \sim \frac{2}{|\tau'(z_0)|} \left(\frac{\pi}{\omega_L \Omega} \right)^{1/2}. \quad (23)$$

It is instructive to compare L_{eff} with a typical coherence length L_c that is observed when the decrease of the laser intensity does not compensate for the difference in the phase velocities. If the amplitude of a selected oscillation of the laser field remains constant during propagation, that is, $f'(z) = 0$, then the coherence length $L_c = \pi / (\Omega |\tau'(z)|)$. The ratio of the two lengths is estimated as

$$\frac{L_{\text{eff}}}{L_c} \sim \left(\frac{4\Omega}{\pi \omega_L} \right)^{1/2} \sim \sqrt{q}, \quad (24)$$

where $q = \Omega / \omega_L$ is a harmonic order. For relatively low-order harmonics, L_{eff} and L_c are comparable, and the effort required to create conditions that satisfy Eq. (18) may not be justified. For very high harmonic orders $q \gg 1$, the SPM-induced increase of the harmonic intensity can exceed a non-SPM one by orders of magnitude.

4. Scaling of conversion efficiency with gas pressure

When coherent build-up of harmonic radiation is limited by the coherence length, the harmonic output oscillates as the gas pressure is increased. In this case, the optimal gas pressure is the one for which the length of the interaction region is equal to the coherence length. The situation changes dramatically if the conditions for perfect phase-matching (SPM) are realized. Indeed, combining Eq. (23) with Eq. (10), we obtain the total harmonic output as

$$|s(z_0) L_{\text{eff}}|^2 \propto \frac{n_a^2}{|\tau'(z_0)|^2} \propto \frac{p^2}{\left| \frac{1}{c} - \frac{1}{v_{\text{ph}}(z_0)} \right|^2}, \quad (25)$$

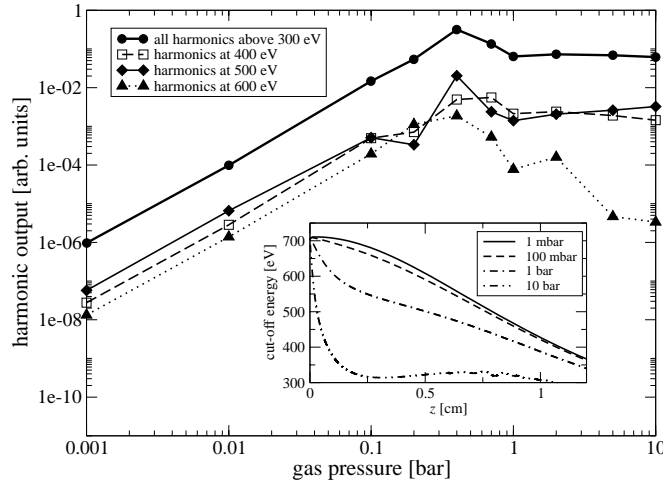


Fig. 4. Scaling of harmonic output with gas pressure p for $\lambda_L = 2.1 \mu\text{m}$. Propagation of the laser pulse was simulated in all spatial dimensions, HHG was simulated on axis only. At small values of p the harmonic output grows quadratically with pressure. Due to SPM, the overall output becomes pressure-independent at large values of p in agreement with Eq. (26). The inset shows the dependence of the cut-off energy on the propagation distance.

where p is a gas pressure and v_{ph} is the phase velocity of the laser light. In jet experiments, the gas pressure is usually high enough for plasma effects to play a significant role in the phase-matching. Otherwise, if p is so small that free electrons hardly affect the propagation of the laser pulse, an increase of the gas pressure would increase the number of radiating dipoles without compromising phase-matching, so that the harmonic output would increase proportionally to p^2 . If the gas pressure is sufficiently large, so that plasma effects start to dominate, $|\tau'(z)|$ becomes proportional to the concentration of free electrons: $|\tau'(z)| \propto n_e$ [26]. In this case, the harmonic output becomes independent of the gas pressure:

$$|s(z_0)L_{\text{eff}}|^2 \propto n_a^2/n_e^2 = \text{const.} \quad (26)$$

This is valid as long as Eq. (18) is satisfied at some point within the jet before the cut-off energy drops below Ω . This is illustrated in Fig. 4. Using the same laser pulse as in Fig. 1, we simulated HHG for different values of p . Propagation started at the focus of the laser beam and stopped after the vacuum Rayleigh length $z_R = 1.24 \text{ cm}$. The overall harmonic output (solid line) was calculated by integrating the harmonic intensity above 300 eV, while harmonic output at selected energies was calculated within a 10-eV-broad Gaussian spectral window. After an initial quadratic growth, the overall harmonic output becomes pressure-independent for $p \gtrsim 1 \text{ bar}$. At the same time, a high gas pressure is detrimental to the harmonic intensity at 600 eV. These harmonics cannot profit from the SPM due to the fast decrease of the cut-off energy at the beginning of propagation.

5. Scaling of conversion efficiency with the laser wavelength

In this section we investigate the regime of moderate ionization rates when the efficiency of HHG is not limited by the ground-state depletion. First of all, we have to decide how to compare HHG at a selected frequency Ω for different laser wavelengths. One obvious possibility is to fix all the laser parameters except λ_L . However, in this case the ratio $\Omega_{\text{cutoff}}/\Omega$ will vary with λ_L . Proceeding this way, we may end up comparing harmonics generated in the cut-off region with

harmonics lying deeply in the plateau region. In our opinion, a fairer comparison is made by fixing the cutoff frequency Ω_{cutoff} , which is equivalent to the requirement that the laser intensity be decreased with decreasing ω_L as ω_L^2 . We also keep the number of cycles and the energy in the laser pulse constant, increasing pulse duration as ω_L^{-1} . In this case, the required decrease of the laser intensity is achieved by increasing the waist of the laser beam as $\omega_L^{-1/2}$.

The scaling of the HHG efficiency is determined by the interplay between the single-atom dipole response and the effective propagation distance L_{eff} , over which radiation from individual atoms is added constructively. As ω_L decreases, lower laser intensities are needed to generate the same Ω_{cutoff} . In the tunneling regime [34], the quasi-static ionization rate is proportional to $\exp[-\frac{2}{3}(2W_b)^{3/2}/|E(t)|]$. Therefore, the density of free electrons n_e rapidly decreases as longer laser wavelengths are used to generate harmonics, for a fixed Ω_{cutoff} . Ionization is a prerequisite of HHG, but free electrons are a major factor limiting coherent harmonic build-up. There are also other factors important for the scaling of conversion efficiency with laser wavelength: depletion of the ground state, spatial spreading of the free electron wave packet, spatiotemporal reshaping of the laser pulse etc. Also, it has recently been demonstrated that scaling predicted by models based on the strong-field approximation may differ from that obtained by a numerical solution of the time-dependent Schrödinger equation [7]. Due to the complexity of these effects, an accurate determination of scaling laws calls for numerical simulations. However, the primary role is played by the dependence of $L_{\text{eff}}^2|\tilde{d}(\Omega)|^2$ on the ionization probability, and in this section we derive a rule-of-thumb scaling law, which roughly describes to which extent an increase of L_{eff} can compensate for the corresponding decrease of the single-atom dipole response.

The magnitude of the contribution from a certain trajectory can be estimated in the same way that we used to estimate its phase: by applying the stationary phase method to calculate the Fourier transform of the single-atom dipole response $d(t)$. In the plateau region, the dependence of the source term (10) on trajectory parameters is given by

$$|s|^2 \propto \frac{n_a(t_b)n_a(t_r)\Gamma(t_b)}{(t_r - t_b)^3 E_L(t_b)^2 |S''(t_r)|}. \quad (27)$$

If the depletion of the ground state is weak, $n_a(t_b)$ and $n_a(t_r)$ are approximately equal to the initial concentration of neutral atoms n_a . The term $(t_r - t_b)^3 E_L(t_b)^2$ describes the spreading of the electron wave packet during its propagation in the continuum, and $\Gamma(t_b)$ is the ionization rate at the appropriate moment of birth. Finally, $S''(t_r) = W'_{\text{kin}}(t_r)$ is the energy chirp of the returning electron wave packet, which scales as the amplitude of the laser field E_0 and limits the time of emission at Ω during a single recollision. Near the cutoff, where $W'_{\text{kin}}(t_r) = 0$, one can show that $W'_{\text{kin}}(t_r)$ has to be replaced with the second-order derivative $[W''_{\text{kin}}(t_r)]^{2/3}$, which scales as $(E_0\omega_L)^{2/3}$. Taking into account that the travel time $t_r - t_b$ scales as ω_L^{-1} , we see that

$$|s|^2 \propto n_a^2 \Gamma(t_b) \omega_L^3 E_0^{-3} \quad (28)$$

in the plateau region of the spectrum, or

$$|s|^2 \propto n_a^2 \Gamma(t_b) \omega_L^3 E_0^{-2} [E_0 \omega_L]^{-2/3} \quad (29)$$

at the cutoff. When the cut-off energy is fixed, $E_0 \propto \omega_L$ and the polynomial frequency-dependent scaling essentially drops out:

$$|s|^2 \propto n_a^2 \Gamma(t_b) \omega_L^{-\delta}, \quad (30)$$

where $\delta = 0$ at the plateau and $\delta = 1/3$ at the cutoff. We ignore this slow dependence below. All frequency dependence has now been shifted into the ionization rate $\Gamma(t_b)$, which very strongly depends on E_0 , the latter decreasing proportionally to ω_L .

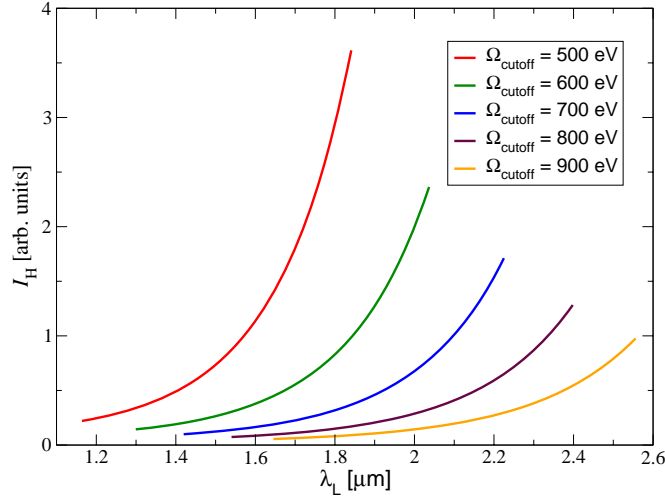


Fig. 5. Scaling law given by Eq. (32). The ionization rate of helium was calculated for a 2-cycle Gaussian laser pulse with a peak intensity adjusted to have a required value of the cut-off energy Ω_{cutoff} . Only simulations with an ionization probability between 0.1% and 10% are shown in this plot.

The scaling of the length of coherent harmonic build-up can be deduced from Eq. (23). When the phase-velocity of the laser light is mainly determined by its interaction with a plasma, $\tau'(z)$ is proportional to n_e/ω_L^2 , so that

$$L_{\text{eff}} \propto \frac{\omega_L^{3/2}}{n_e} \propto \frac{\omega_L^{5/2}}{n_a \Gamma(t_b)}. \quad (31)$$

Here we used $n_a \Gamma(t_b) \propto \omega_L n_e$, assuming a moderate ionization probability (the number of ionized atoms is proportional to the rate of tunneling ionization multiplied with the time during which tunneling remains an efficient ionization channel).

Eqs. (30) and (31) finally provide a scaling law for the harmonic intensity:

$$I_H \propto |s|^2 L_{\text{eff}}^5 \propto \frac{\omega_L^5}{\Gamma(t_b)}. \quad (32)$$

Both the numerator and the denominator of the last expression decrease as the laser wavelength λ_L is increased, but if the laser intensity is simultaneously decreased in order to keep the cut-off energy fixed, then $\Gamma(t_b)$ in the denominator decreases exponentially, while the numerator decreases polynomially. Longer wavelength radiation is indeed more sensitive to plasma dispersion, but the decrease in plasma density compensates for it, increasing the length L_{eff} and the overall conversion efficiency.

The scaling law given by Eq. (32) is illustrated in Fig. 5. As an estimation of the ionization rate at the moment of birth $\Gamma(t_b)$, we used the peak ionization rate of the half-cycle, within which the cut-off trajectory of a two-cycle Gaussian pulse is launched. Quasi-static ionization rates [22] were used to calculate $\Gamma(t)$.

6. Summary

We investigated the role of propagation effects in the generation of soft X-ray harmonics by few-cycle laser pulses. Our analytical theory, based on the Lewenstein model of HHG and

supported by numerical simulations, reveals that increasing the wavelength of the driving field brings several important opportunities for the generation of isolated attosecond pulses in this spectral region: Conditions for ideal phase-matching (SPM) can be fulfilled even with moderate ionization rates when the blue-shift is negligible. It is possible to tune parameters such that only one attosecond burst benefits from this regime, in which case the intensity of the burst may exceed the intensities of other bursts by orders of magnitude. Consequently, generation of a single attosecond pulse in the soft X-ray region does not necessarily require a careful extraction of the cut-off region. Also, the efficiency of generation of soft X-ray harmonics can be improved by using a driving field with a longer wavelength. We hope that our theory will serve as a guideline for future HHG experiments with phase-stabilized few-cycle mid-infrared pulses.

Acknowledgments

Supported by Deutsche Forschungsgemeinschaft through the DFG-Cluster of Excellence Munich-Centre for Advanced Photonics (MAP). M.I. acknowledges support from the Bessel prize of the A. v. Humboldt foundation, the hospitality of the Max-Planck Institute for Quantum Optics, and NSERC support via SRO grant SROPJ 299409-03r. V.S.Y. thanks Dr. Valer Tosa for many useful discussions and his unpublished simulations that triggered this research.